Original Article

Dynamic ^{68}Ga-DOTA^{0}-Tyr^{3}-octreotate positron emission tomography-computed tomography for the evaluation of pancreatic neuroendocrine tumors: a pilot study

Hongyan Yin[#], Guobing Liu[#], Hui Tan, Dai Shi, Dengfeng Cheng, Haojun Yu, Hongcheng Shi

Department of Nuclear Medicine, Zhongshan Hospital, Fudan University, Shanghai, China

Contributions: (I) Conception and design: H Yin, G Liu, H Shi; (II) Administrative support: D Cheng, H Yu, H Shi; (III) Provision of study materials or patients: H Yin, G Liu, D Cheng; (IV) Collection and assembly of data: H Yin, G Liu, H Tan, D Shi, H Yu; (V) Data analysis and interpretation: H Yin, G Liu, H Tan, D Shi; (VI) Manuscript writing: All authors; (VII) Final approval of manuscript: All authors.

[#]These authors contributed equally to this work.

Correspondence to: Hongcheng Shi, MD, PhD. Department of Nuclear Medicine, Zhongshan Hospital, Fudan University, No. 180 Fenglin Road, Shanghai 200032, China. Email: shi.hongcheng@zs-hospital.sh.cn.

Background: ^{68}Ga-DOTA^{0}-Tyr^{3}-octreotate (^{68}Ga-DOTATATE) is a radiolabeled somatostatin analog used for the diagnosis of pancreatic neuroendocrine tumors (pNETs), and standardized uptake value (SUV) measurements for therapeutic monitoring is recommended. However, changes in net influx rate (K_i) may better reflect treatment effects than may those of the SUV. The aim of this study was to investigate the value of dynamic ^{68}Ga-DOTATATE positron emission tomography-computed tomography (PET-CT) in the evaluation of pNETs.

Methods: Dynamic PET-CT scans over 60 min were acquired for 7 patients with localized pancreatic mass before surgery. Maximal and mean SUV (SUV_{max} and SUV_{mean}) were measured in tumors and normal pancreatic body as reference tissue (RT). Time-activity curves (TACs) were extracted from tumors and RT. A 2-tissue compartment model was used to calculate the rate constants K_1, k_2, and k_3 (min^{-1}); K_i (mL/g/min); and K_1:k_2 ratio. The following statistical tests were used to evaluate the results: the Shapiro-Wilk, Student t test, Mann-Whitney, Spearman, and Pearson rank correlation tests.

Results: Among 6 patients, 8 primary tumors were histopathologically proven to be pNETs. Moreover, 6 lesions with high uptake of ^{68}Ga-DOTATATE showed an ascending TAC pattern, while 2 lesions with no or low uptake showed a descending TAC pattern. The mean SUV_{max} and SUV_{mean} of pNETs were 46.4±40.2 (range, 3.9–109.9) and 21.9±16.0 (range, 0.5–42.8), respectively, which were significantly higher than the SUV_{max} of 4.2±0.6 (range, 3.1–4.9) and the SUV_{mean} of 2.7±1.0 (range, 1.4–3.6) for the RT (P=0.021 and P=0.036), respectively. The K_i of pNETs was statistically higher than that of the RT [pNET: 0.366±0.372 (range, 0.019–0.992); RT: 0.060±0.017 (range, 0.04–0.08); P=0.036]. The mean K_1:k_2 ratio in pNETs was 12-fold higher than that of RT (6.06 *vs.* 0.50). In pNETs, there was a positive correlation between SUV_{max} and K_i (r=0.952; P<0.001) and between SUV_{mean} and K_i (r=0.905; P=0.002). Another patient was diagnosed with intrapancreatic accessory spleen.

Conclusions: The uptake of ^{68}Ga-DOTATATE by pNETs can be explained by its high K_i value and K_1:k_2 ratio. Dynamic ^{68}Ga-DOTATATE PET-CT can serve as a potential tool for evaluating pNETs and support the further assessment of a larger cohort of patients.

Keywords: ^{68}Ga-DOTA^{0}-Tyr^{3}-octreotate (^{68}Ga-DOTATATE); positron emission tomography-computed tomography (PET-CT); dynamic imaging; pancreatic neuroendocrine tumor

Submitted Sep 20, 2022. Accepted for publication Jun 05, 2023. Published online Jul 07, 2023.
doi: 10.21037/qims-22-998
View this article at: https://dx.doi.org/10.21037/qims-22-998

Introduction

Neoplasms of the pancreatic endocrine tissues, known as pancreatic neuroendocrine tumors (pNETs), are extremely rare and heterogeneous. It is estimated that the incidence of pNETs is approximately 1/100,000 (1,2), but recently, it has increased significantly. Depending on whether pNETs release hormones, such as insulin, gastrin, glucagon, and vasoactive intestinal peptide, they can be classified as functioning or nonfunctioning, resulting in a variety of clinical syndromes. Approximately 60% to 90% of pNETs are nonfunctioning and generally asymptomatic (3). Due to the relative rarity of pNETs and nonspecific symptoms, patients are often diagnosed with advanced disease. The only curative treatment option for localized pNETs is surgery (4). Patients with locally resected pNETs have a 5-year survival rate of 55%, while patients with nonresectable pNETs have a 5-year survival rate of 15% (5). Thus, improving the prognosis of pNETs requires early diagnosis.

Imaging studies are vital to the diagnosis and treatment of pNETs. The most common imaging method is computed tomography (CT), particularly for the purpose of staging and differential diagnosis. In contrast to the CT scan, magnetic resonance imaging (MRI) involves less radiation exposure and may have a higher sensitivity in detecting small lesions or liver metastases in the pancreas (6). The most sensitive test for localizing small pNETs is endoscopic ultrasonography, which also allows for a biopsy through fine needle aspiration to confirm the diagnosis (7). Somatostatin receptors (SSTRs) are expressed by 80–100% of pNETs (8). Positron emission tomography-computed tomography (PET-CT) with ^{68}gallium-labeled somatostatin analog (^{68}Ga-SSA) is the most sensitive method for the detection of pNETs (9). A timely prediction of treatment response is vital in helping guide tumor therapy and avoiding unnecessary side effects and costs associated with ineffective therapies.

Standardized uptake value (SUV) is the most commonly used method to quantify SSTR expression in neuroendocrine tumors (NETs) (10-13). A study by Gabriel *et al.* (11) on ^{68}Ga-DOTA^0-Tyr^3-octreotide (^{68}Ga-DOTATOC) PET-CT findings revealed that changes in tumor maximal SUV (SUV_{max}) between baseline and follow-up did not correlate with the outcome of treatment with peptide receptor radionuclide therapy. Additionally, Haug *et al.* (10) reported similar findings: in assessing the response to peptide receptor radionuclide therapy, changes in tumor-to-spleen SUV ratio between baseline and follow-up ^{68}Ga-DOTA^0-Tyr^3-octreotate (^{68}Ga-DOTATATE) were more accurate than were changes in tumor SUV_{max}. In a study on the kinetic parameters of ^{68}Ga-DOTATOC and ^{68}Ga-DOTATATE, Velikyan *et al.* (14) found that the kinetic parameter net influx rate (K_i) based on dynamic scan might provide a more accurate measurement tool for the evaluation of therapy response.

Dynamic ^{68}Ga-SSA PET-CT studies have focused on meningiomas (15), non-small cell lung cancers (16), and metastatic neuroendocrine tumors (14,17-20), with the enrolled sample sizes ranging from 9 to 22 due to the low incidence of NETs. Moreover, little research has been conducted on ^{68}Ga-SSA dynamic PET-CT imaging for pNETs. A recent study showed that K_i based on dynamic ^{68}Ga-DOTATOC PET-CT exhibited the best diagnostic performance (sensitivity 88.5%, specificity 94.4%, accuracy 90.9%) in identifying the physiological uptake of pancreatic uncinate process and pNETs (21). There, we conducted a study whose objective study was to determine the value of dynamic ^{68}Ga-DOTATATE PET-CT in the evaluation of pNETs.

Methods

Participants

This study was conducted in accordance with the Declaration of Helsinki (as revised in 2013) and was approved by the institutional review board of Zhongshan Hospital (No. IRB-B2020-186R). All consecutive patients provided written informed consent before entering the study from August 2020 to October 2021. We conducted a prospective pilot study to investigate the value of dynamic ^{68}Ga-DOTATATE PET-CT in localized pancreatic mass. The inclusion criteria were as follows: (I) patients willing to undergo 60-min dynamic PET, (II) patients who had undergone contrast-enhanced MRI or CT scans, (III) patients who had not received any previous treatment, (IV) patients who had undergone resection of the lesion

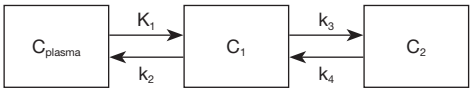

Figure 1 Diagram of the tracer kinetics of ^{68}Ga-DOTATATE. A 2-tissue compartment model is used. K_1 describes the binding to the receptor, k_2 the displacement from the receptor, k_3 the cellular internalization, and k_4 the externalization. ^{68}Ga-DOTATATE, ^{68}Ga-DOTA^0-Tyr^3-octreotate.

for histopathological evaluation within 4 weeks following PET-CT scans, and (V) patients with the ability to provide written informed consent. The patients underwent PET-CT without any contraindications. The size of the lesion was based on the measurement of the surgical specimen.

Dynamic PET-CT imaging and reconstruction

The preparation of ^{68}Ga-DOTATATE was carried out as described previously (22). The study was conducted with a total-body PET-CT scan using an axial field of view of 194 cm (uEXPLORER, United Imaging Healthcare, Shanghai, China). First, a low-dose CT scan was performed (120 kVp; 10 mAs) in order to correct attenuation. Then, following a bolus injection of 60.0–83.3 MBq ^{68}Ga-DOTATATE into a vein near the ankle, a 60-minute dynamic PET scan was performed. Upon completion of the dynamic acquisition, a diagnostic CT scan was performed (120 kVp; automatic tube current modulation with dose level range, from 1 to 5 and mAs range, from 4 to 432). A number of corrections were made to the PET images with regard to attenuation, scatter, alignment, decay, normalization, and randoms. After this, they were reconstructed using a list-mode ordered subsets expectation maximization algorithm (3 iterations, 20 subsets), which included time-of-flight and point-spread-function modeling in combination with a 3.0-mm Gaussian filter. The matrix size of image was 192×192 pixels. We divided the dataset into 55 frames (36×5 s and 19×180 s).

Data analysis

Images were analyzed qualitatively in the axial, coronal, and sagittal views. According to qualitative visual assessment, lesions of interest were considered positive when avidity was greater than the background in areas without physiological uptake.

Semiquantitative analysis was conducted using the volume of interest (VOI) and SUV calculations. On the axial section of the fused PET-CT scan, a VOI was created at an anatomic level corresponding to known pancreatic masses, and the VOI was manually adjusted to encompass the maximum available lesion size in all 3 planes. Two additional VOIs were defined in relation to the descending aorta as the mediastinal blood pool (2.0 cm in diameter), with normal pancreatic parenchyma being used as the reference tissue (RT, 1.5 cm in diameter). SUV (50–60 min post-injection) was calculated as the tissue concentration of tracer per injected tracer dose per body weight. The SUV_{max} and mean SUV (SUV_{mean}) of the pancreatic mass, RT, and mediastinum were measured. In order to calculate the tumor-to-mediastinum tissue ratio (TMR), the SUV_{mean} of the tumor was divided by the SUV_{mean} of the mediastinum. The tumor-to-pancreas tissue ratio (TPR) was defined as the SUV_{mean} of the tumor divided by the SUV_{mean} of the pancreas.

A vendor-provided workstation (uWS-MI R001; United Imaging Healthcare) was used to analyze the reconstructed PET and CT images. On the summation image of the dynamic examination, VOIs were drawn over the pancreatic masses, the RT, and an arterial vessel, and then projected onto all time frames to generate time-activity curves (TACs). For the appropriate placement of VOIs, CT and/or MR images were used. TAC patterns were classified 3 phases based on their characteristics: initial phase, 1 min after administration of ^{68}Ga-DOTATATE; early phase, 1 to 10 min after administration of ^{68}Ga-DOTATATE, where rapid changes are observed; and late phase, 10 min after administration of ^{68}Ga-DOTATATE, when slow changes can be observed.

Due to the fixed location in the posterior mediastinum and being less spillover from adjacent organs, the VOIs in the descending aorta were automatically drawn to obtain the input function. By uploading the TAC data to PMOD version 3.2 (PMOD Technologies Ltd., Zurich, Switzerland) (15,18,19), a quantitative analysis of the dynamic data was performed. Based on previous studies, a 2-compartment model was used for model fitting (15,18,19). The rate constants K_1, k_2, and k_3 (min^{-1}); K_i (mL/g/min); and the K_1:k_2 ratio were calculated. *Figure 1* illustrates the compartmental configuration of this model. K_1 is associated with the binding of receptor, k_2 with the displacement from the receptor, k_3 with the internalization of cells, and k_4 with the externalization of cells. This study did not analyze k_4 since it is typically close to 0.

Table 1 Patients characteristics

Patient no.	Lesion no.	Sex	Age (years)	Injected dose (MBq)	Location	SUV_{max}	SUV_{mean}	Surgery	Pathology	K_i-67 index	Miotic rate (10HPF)	SSTR2	SSTR5	Size (cm)
1	1	Male	43	81.8	Head	57.3	24.0	RPD	NET G1	2%	1	/	/	2.0
2	2	Male	63	83.3	Head	109.9	42.8	RPD	NET G2	5%	1	/	/	1.8
	3				Tail	97.2	42.1	PTTR	NET G2	5%	1	100%+++	100%++	3.0
3	4	Female	52	60.0	Head	46.1	27.1	PHTR	NET G1, insulinoma	1%	<2	100%++	100%+	1.0
	5				Body and tail	35.5	23.9	DPS	NET G1	1%	<2	100%+++	100%+	0.7
4	6	Male	55	73.7	Head	16.9	11.5	RPD	NET G2, insulinoma	2%	2	/	/	2.0
5	7	Female	48	61.9	Tail	4.4	3.1	DPS	NET G2, insulinoma	5%	3	10%+	–	0.8
6	8	Female	49	66.4	Head	3.9	0.5	RPD	NET G2	3%	1	5%++	90%++	8.0

SUV_{max}, maximal standardized uptake value; SUV_{mean}, mean standardized uptake value; RPD, radical pancreaticoduodenectomy; PTTR, pancreatic tail tumor resection; PHTR, pancreatic head tumor resection; DPS, distal pancreatectomy with splenectomy; NET, neuroendocrine tumor; G1, grade 1; G2, grade 2; SSTR, somatostatin receptor.

Postoperative histopathologic analysis

In this study, all patients with pancreatic lesions had the lesion resected within 4 weeks following PET-CT scans. Histopathologic confirmation was performed in pNETs. Histopathology was reviewed by 2 experienced pathologists. Based on the number of mitoses per 10 high-power fields and the K_i-67 index (percentage of positive cells in areas of higher nuclear labeling), pathological tumor grades were determined as per the World Health Organization (WHO) classification.

Statistical analysis

In order to conduct statistical analyses, SPSS software version 23.0 (IBM Corp., Armonk, NY, USA) was used. Data are expressed as mean ± standard deviation. An assessment of normality was conducted using the Shapiro-Wilk test. In comparing the groups, the Student *t* test was used for variables with a normal distribution, while the Mann-Whitney test was used for variables without a normal distribution. For assessment of the relationship, Pearson and Spearman rank correlation analyses (for normal and nonnormal distributions, respectively) were conducted. All P values reported were 2-sided, and significance was set at a P value less than 0.05.

Results

Study group

The study included 7 patients with pancreatic mass who underwent dynamic ^{68}Ga-DOTATATE PET-CT. For histopathologic confirmation, surgical intervention was performed in all patients, including 4 with single pNETs, 2 with double pNETs, and 1 with intrapancreatic accessory spleen (IPAS). *Table 1* summarizes the characteristics of the participants with pNETs (6 patients with 8 tumors), comprising 3 men and 3 women with a mean age of 51.7 (range, 43–63) years. Five tumors were located in the head of pancreas, and three in the tail. Three functional pNETs were all insulinomas, and the remainder were nonfunctional pNETs. ^{68}Ga-DOTATATE uptake above the normal pancreatic level was observed in 6 of the 8 lesions. According to the 2019 WHO classification criteria for gastroenteropancreatic neuroendocrine tumors, all tumors were well-differentiated neuroendocrine tumors (grade 1 and grade 2). Immunolabeling was consistently detected in pNETs for SSTR2 and SSTR5 (5/8 lesions, 62.5%). Three lesions showed a high rate of SSTR2 expression, and two lesions showed a low rate. The mean SUV_{max} (59.6) and SUV_{mean} (31.0) of lesions with a high rate of SSTR2 expression were higher than those with a low rate (mean SUV_{max} of 4.2, mean SUV_{mean} of 1.8). A single non-

neuroendocrine mass was consistent with IPAS in the pancreatic tail; however, both preoperative conventional imaging (enhanced CT and MRI) and ^{68}Ga-DOTATATE PET-CT were suggestive of pNET.

Characteristics of ^{68}Ga-DOTATATE PET-CT imaging and TACs

Based on the visual evaluation of the ^{68}Ga-DOTATATE scans, it was observed that there was increased uptake in 6 of the 8 pNETs. Two lesions were not delineated on the ^{68}Ga-DOTATATE study. The TAC patterns could be divided into 4 types (*Figure 2*): curve pattern type 1 (*Figure 2A*) exhibited a low or middle level in the initial phase, a rapid rise in the early phase, and a continuous rise in the late phase; curve pattern type 2 (*Figure 2B*) showed a low or middle level in the initial phase, a transient decrease between 1 to 3 min followed by rapid increase after 3 min of the early phase, and a slow increase in the late phase; curve pattern type 3 (*Figure 2C*) showed a low level in the initial phase, a rapid decline in the early phase, and a consistent or slow decline in the late phase; and curve pattern type 4 (*Figure 2D*) showed a low level in the initial phase, a rapid decline in the early phase, and a continuous decline in the late phase. Two tumors appeared as curve pattern type 1, four as curve pattern type 2, one as curve pattern type 3, and one as curve pattern type 4. PET-positive pNETs exhibited an ascending curve, while PET-negative pNETs showed a descending curve.

The 3 functional pNETs were all insulinomas, and 2 tumors were detected on ^{68}Ga-DOTATATE (*Figure 3*), while 1 was not detected (*Figure 2C*). All patients had symptoms of hypoglycemia. The average size of the insulinomas was 1.3±0.5 cm (range, 0.8–2.0 cm), and the mean SUV_{max} was 22.5±17.5 (range, 4.4–46.1). The TAC of the PET-positive insulinomas showed as curve pattern type 2, but that of PET-negative insulinomas appeared as curve pattern type 3.

IPAS and accessory spleen (*Figure 4*) showed mild-to-strong ^{68}Ga-DOTATATE uptake. TACs of IPAS and accessory spleen appeared as ascending curves, which were similar to that of PET-positive pNETs but different from that of normal pancreatic tissue.

Static and dynamic imaging parameters of pNETs and reference tissue

For normal pancreatic tissue, ^{68}Ga-DOTATATE tends to show moderate uptake (23). In our study, the mean SUV_{max} and SUV_{mean} of RT were 4.2±0.6 (range, 3.1–4.9) and 2.7±1.0 (range, 1.4–3.6), respectively, while the mean SUV_{max} and SUV_{mean} of pNETs were 46.4±40.2 (range, 3.9–109.9) and 21.9±16.0 (range, 0.5–42.8), respectively. The largest lesion was located in the pancreatic head of patient 6 (8.0 cm in diameter), and the smallest lesion was in the pancreatic tail of patient 3 (0.7 cm in diameter). *Table 1* presents the SUV and lesion size in pNETs, and these parameters did not demonstrate a correlation. In pNETs, the SUV_{max} and SUV_{mean} were significantly higher than those RT (P=0.021 and P=0.036), as shown in *Figure 5A,5B*.

In terms of K_i, there was a statistically significant difference between pNETs and RT (pNET: 0.366; RT: 0.060; P=0.036), as shown in *Figure 5C*. However, pNETs and RT were not significantly different in terms of K_1 (1.371 *vs.* 1.424), k_2 (2.076 *vs.* 2.939), or k_3 (0.273 *vs.* 0.135). The mean and standard deviation are given in *Table 2*. There was a 12-fold increase in the mean K_1:k_2 ratio in pNETs compared to that of RT (6.06 *vs.* 0.50).

In pNETs, the SUV_{max}, SUV_{mean}, TPR, TMR, and K_i were positively correlated (r=0.952, P<0.001; r=0.905, P=0.002; r=0.881, P=0.004; r=0.905, P=0.002), as shown in *Figure 6*. No correlations between SUV_{max} or SUV_{mean} and K_1, k_2, or k_3 were detected in pNETs.

Discussion

This study explores the potential role of dynamic ^{68}Ga-DOTATATE PET in the assessment of pNETs. First, 6 of 8 pNETs exhibited an ascending curve, whereas 2 pNETs showed a descending curve. Second, the SUV_{max}, SUV_{mean}, K_i, and K_1:k_2 ratio of pNETs were higher than those RT. Hence, the uptake of ^{68}Ga-DOTATATE by pNETs can be explained by high K_i and K_1:k_2 ratio. Finally, K_i, SUV_{max}, SUV_{mean}, TPR, and TMR were all positively correlated. Thus, dynamic PET studies can serve as a potential tool for evaluating pNETs. Further research may enable the monitoring of SSTRs of pNETs based on these data.

In a retrospective study on the diagnostic performance of ^{68}Ga-DOTATATE in NETs (24), a total of 728 patients and 1258 PET-CT images were included, with the results indicating that ^{68}Ga-DOTATATE PET-CT has high sensitivity for the localization of NETs (>94%) and specificity (>92%). In this study, 6 of 8 pNETs could be delineated with enhanced ^{68}Ga-DOTATATE uptake in comparison to the adjacent pancreatic parenchyma, and 3 of the lesions were stained with SSTR2 and showed

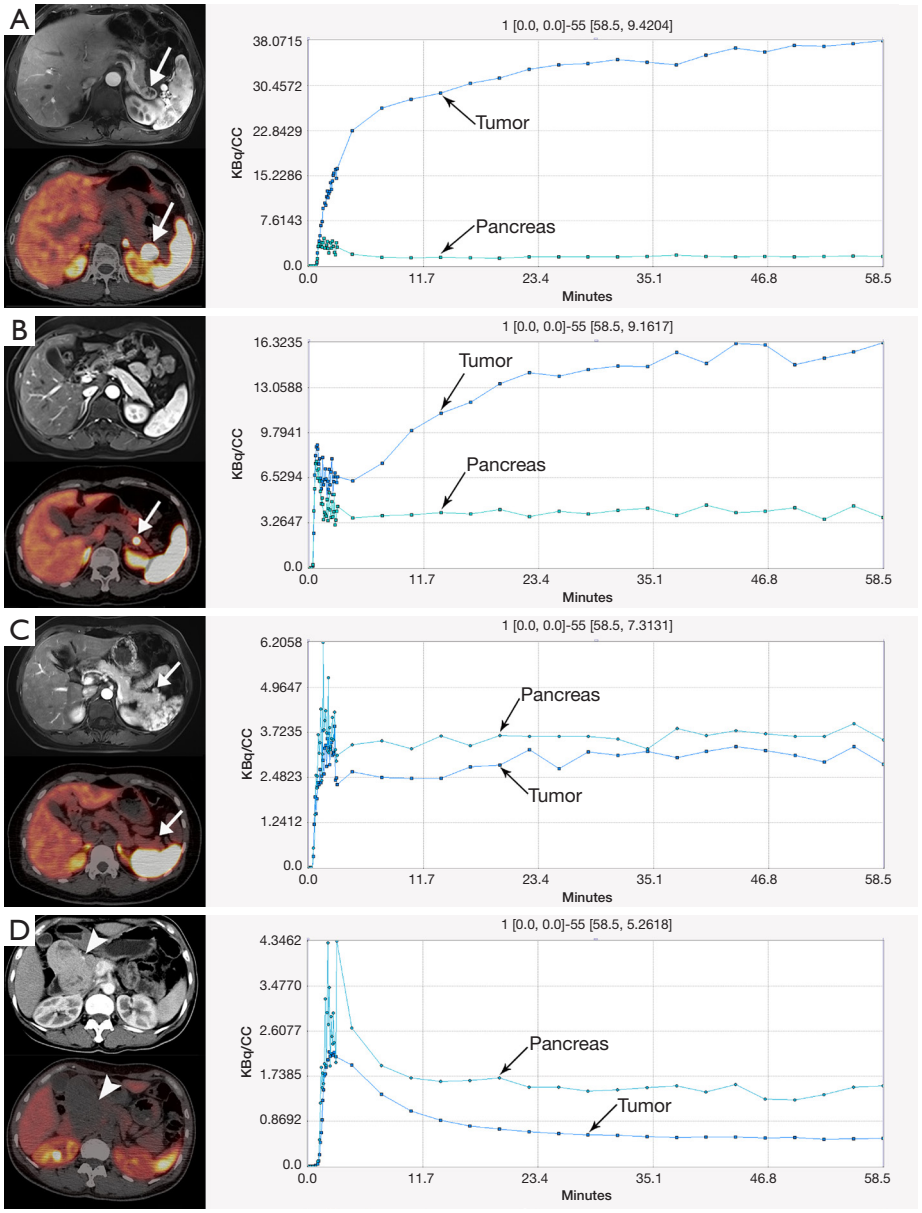

Figure 2 Examples of ^{68}Ga-DOTATATE kinetics. (A-C, left upper) Contrast-enhanced T1-weighted MRI and (D, left upper) contrast-enhanced CT. (A-D, left lower) Fusion PET-CT showing ^{68}Ga-DOTATATE uptake from 50 to 60 min p.i. (A-D, right) time-activity curves of tumor and normal pancreatic tissue. (A) Curve pattern type 1 (pNET grade 2; patient 2, lesion 3) showed a low or middle level in the initial phase, a rapid increase in the early phase, and a continuous increase in the late phase (thin arrow). The tumor was heterogeneously contrast enhanced (thick arrow). (B) Curve pattern type 2 (pNET grade 1; patient 3, lesion 5) showed a low or middle level in the initial phase, a transient decrease between 1 to 3 min, followed by rapid increase after 3 min of the early phase, and a slow increase in the late phase (thin arrow). The tumor was not visualized on the contrast-enhanced MR images. (C) Curve pattern type 3 (pNET grade 2, insulinoma; patient 5) showed a middle level in the initial phase, a rapid decrease in the early phase, and a consistent or limited/slow decrease in the late phase (thin arrow). The tumor was homogeneously contrast enhanced (thick arrow). (D) Curve pattern type 4 (pNET grade 2; patient 6) showed a middle level in the initial phase, a rapid decrease in the early phase, and a continuous decrease in the late phase (thin arrow). The tumor was heterogeneously contrast enhanced (arrowhead). ^{68}Ga-DOTATATE, ^{68}Ga-DOTA^{0}-Tyr^{3}-octreotate; MRI, magnetic resonance imaging; CT, computed tomography; PET-CT, positron emission tomography-computed tomography; pNET, pancreatic neuroendocrine tumor.

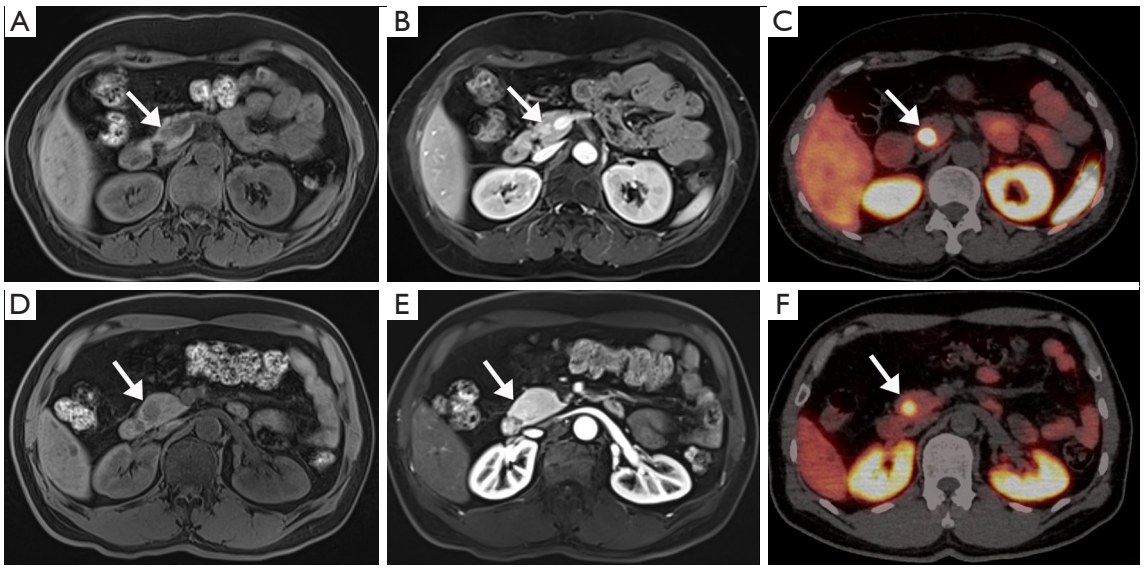

Figure 3 Well-differentiated syndromic pNETs (insulinomas). (A-C) Patient 3, lesion 4. (D-F) Patient 4. (A,D) Noncontrast T1-weighted MR images showed a hypointense tumor in the pancreatic head (arrows), (B,E) with homogeneous hyperenhancement being found in the subsequent contrast-enhanced T1-weighted images (arrows). (C,F) The tumors showed intense uptake of ^{68}Ga-DOTATATE in the PET-CT fusion images (arrows). pNETs (insulinomas) were confirmed by histologic results. pNETs, pancreatic neuroendocrine tumors; MR, magnetic resonance; ^{68}Ga-DOTATATE, ^{68}Ga-DOTA^{0}-Tyr^{3}-octreotate; PET-CT, positron emission tomography-computed tomography.

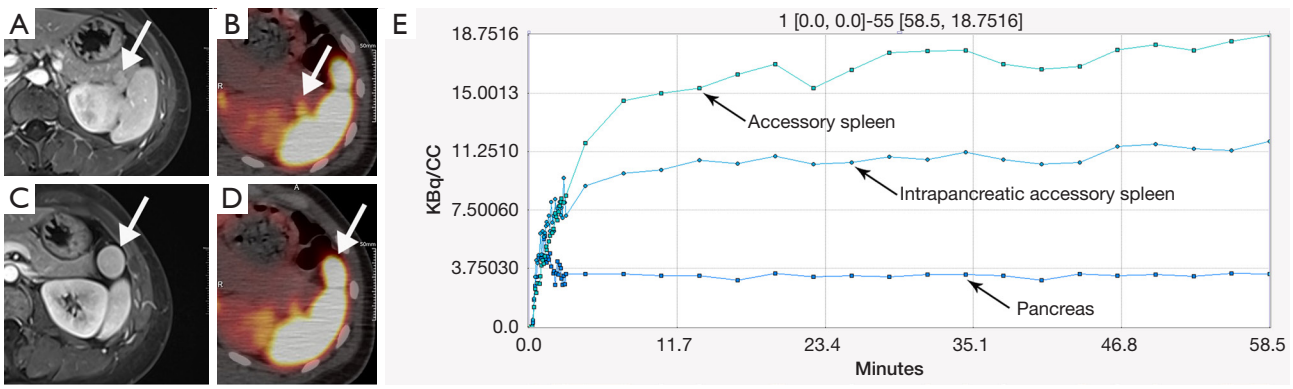

Figure 4 IPAS and accessory spleen. (A) A contrast-enhanced T1-weighted MR image showed contrast enhancement in the nodule of the pancreatic tail (thick arrow). (B) The tumor showed a moderate uptake of ^{68}Ga-DOTATATE in the PET-CT fusion image (thick arrow). pNET was diagnosed before surgery, but histologic results after surgery indicated IPAS. (C) A contrast-enhanced T1-weighted MR image showed contrast enhancement in the nodule of the splenic hilum (thick arrow). (D) The tumor showed an intense uptake of ^{68}Ga-DOTATATE in the PET-CT fusion image (thick arrow). Accessory spleen was diagnosed based on the imaging features and clinical information. (E) Time-activity curves showed that the curve pattern of IPAS was similar to accessory spleen but different from that of the pancreas (thin arrows). IPAS, intrapancreatic accessory spleen; MR, magnetic resonance; ^{68}Ga-DOTATATE, ^{68}Ga-DOTA^{0}-Tyr^{3}-octreotate; PET-CT, positron emission tomography-computed tomography.

high expression. However, the other 2 pNETs were not delineated on the ^{68}Ga-DOTATATE study and presented low SSTR2 expression. The increased uptake of ^{68}Ga-DOTATATE in lesions with high SSTR2 expression was demonstrated by a higher mean SUV_{max} and SUV_{mean} compared with those of lesions with low SSTR2 expression.

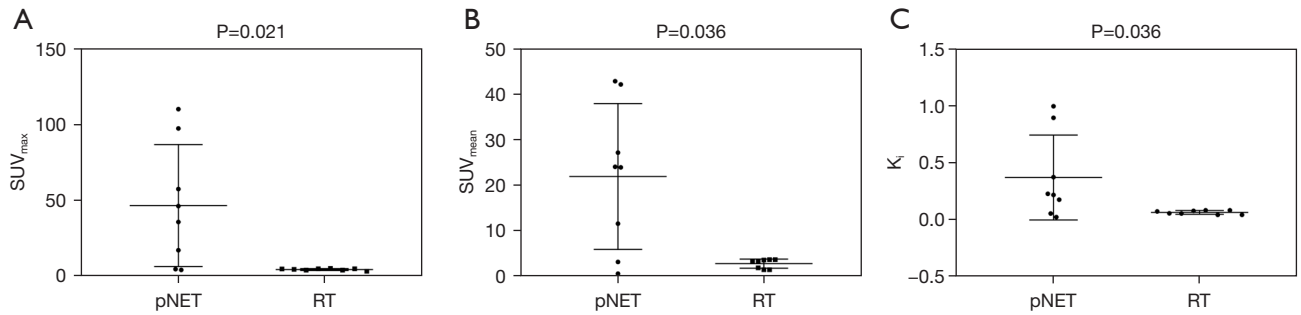

Figure 5 The SUV_{max}, SUV_{mean}, and K_i in pNET lesions were significantly higher than those of normal pancreatic RT. (A) The comparison of SUV_{max} between pNET and RT. (B) The comparison of SUV_{mean} between pNET and RT. (C) The comparison of K_i between pNET and RT. SUV_{max}, maximal standardized uptake value; SUV_{mean}, mean standardized uptake value; K_i, net influx rate; pNET, pancreatic neuroendocrine tumor; RT, reference tissue.

Table 2 Mean values, SDs, and ranges for K_1, k_2, k_3, and K_i for RT and pNETs

Parameter	RT			pNET			P
	Mean	SD	Range	Mean	SD	Range	
K_1	1.424	0.379	0.97–1.994	1.371	0.598	0.507–2.1	0.838
k_2	2.939	0.873	1.778–4.068	2.076	1.988	0.067–4.605	0.113
k_3	0.135	0.055	0.068–0.193	0.273	0.209	0.035–0.588	0.069
K_i	0.060	0.017	0.04–0.08	0.366	0.372	0.019–0.992	0.036
SUV_{max}	4.2	0.6	3.1–4.9	46.4	40.2	3.9–109.9	0.021
SUV_{mean}	2.7	1.0	1.4–3.6	21.9	16.0	0.5–42.8	0.036

SD, standard deviation; RT, reference tissue; pNET, pancreatic neuroendocrine tumor; SUV_{max}, maximal standardized uptake value; SUV_{mean}, mean standardized uptake value.

These findings were also observed in several other studies (25,26), verifying the concordance and correlation between ^{68}Ga-SSA PET-CT and SSTR immunohistochemistry. Moreover, ^{68}Ga-DOTATATE PET-CT even found a small lesion (0.7 cm in diameter), which was missed on the enhanced CT and MR images. However, enhanced CT and MR images can provide important information for lesion characterization for ^{68}Ga-DOTATATE–negative tumor. In patient 6, the pancreatic head lesion up to 8 cm in diameter did not take up ^{68}Ga-DOTATATE on static imaging at 50–60 min, and the TAC of this lesion (*Figure 2D*) indicated that the tumor was transiently perfused after the tracer was injected. It was then gradually excreted, but static imaging can only capture tracer uptake at a single time and cannot reflect dynamic changes. Meanwhile, tumor immunohistochemical indicators showed that SSTR5 was mainly expressed on the surface of tumor cells, but only a small amount of SSTR2 was expressed. ^{68}Ga-DOTATATE is typically combined with SSTR2 (27), so this lesion did not take up ^{68}Ga-DOTATATE.

Insulinoma is the most common functional pNET, originating from the neuroendocrine islet cells (28). Insulinomas are mostly benign, but approximately 5% to 15% are malignant (29). Almost all benign insulinomas express glucagon-like peptide-1 receptor on the cell surface with high incidence and high density (30). Conversely, malignant insulinomas often express SSTR2 (31,32). Insulinomas are usually small in size but life-threatening, and thus preoperative localization and accurate assessment of the extent of all lesions are important. A total of 3 insulinomas were found in this study, all of which were less than 2 cm in diameter. Among them, 3 tumors could be delineated with enhanced ^{68}Ga-DOTATATE uptake, whereas the other one was not delineated. A recent study showed that ^{68}Ga-DOTATATE PET-CT could successfully localize insulinomas in 9 patients out of 10 (33). However, ^{68}Ga-SSA

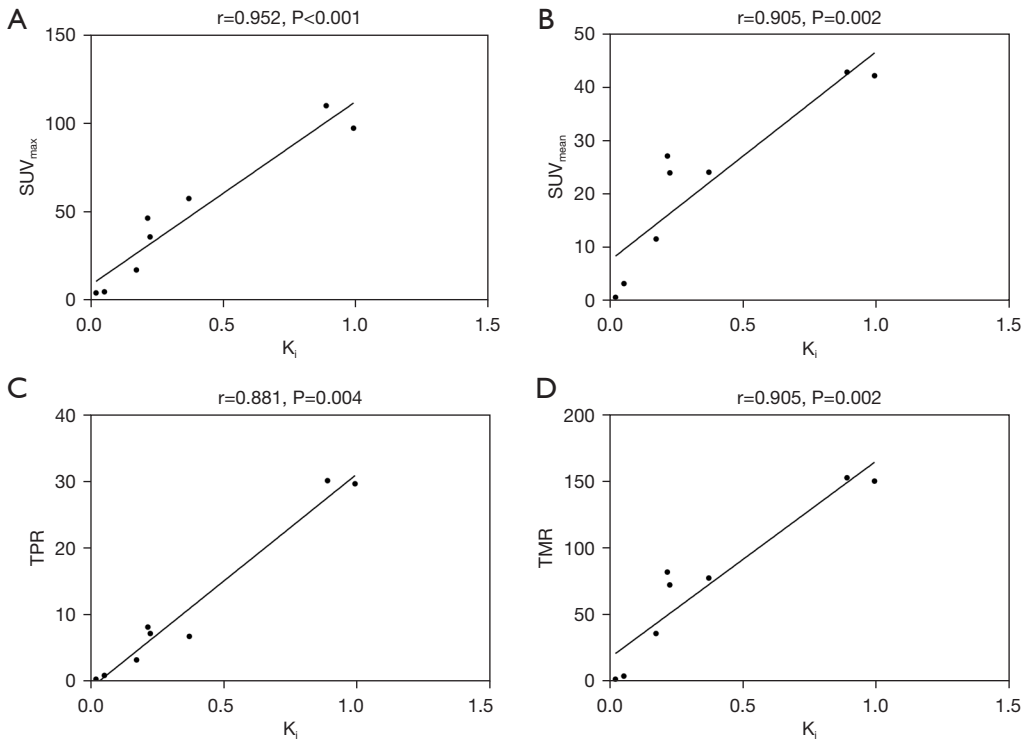

Figure 6 SUV_{max}, SUV_{mean}, TPR, and TMR positively correlated with K_i. (A) The correlation of SUV_{max} and K_i. (B) The correlation of SUV_{mean} and K_i. (C) The correlation of TPR and K_i. (D) The correlation of TMR and K_i. SUV_{max}, maximal standardized uptake value; SUV_{mean}, mean standardized uptake value; TPR, SUV_{mean} tumor to SUVmean pancreas ratio; TMR, SUV_{mean} tumor to SUV_{mean} mediastinum ratio; K_i, net influx rate.

PET has a low sensibility of 25–31% because insulinomas show a low expression of SSTR2 (34). In the prospective study conducted by Luo *et al.* (35), ^{68}Ga-NOTA-exendin-4 PET-CT targeting glucagon-like peptide-1 receptor showed a sensitivity of 97.7% in detecting insulinomas. Glucagon-like peptide-1 receptor imaging and SSTR imaging are complementary in localizing insulinomas.

Dynamic imaging can observe the change process of the tracer distribution in the body, and TAC can better reflect the changing trend, which is helpful for distinguishing benign and malignant diseases. Wang *et al.* (36) found that TAC of malignant pulmonary lesions demonstrated gradually increasing TAC, whereas benign lesions exhibited gradually decreasing curves, which was useful in the differential diagnosis of pulmonary lesions using dynamic ^{18}F-fluorodeoxyglucose (^{18}F-FDG) PET-CT. In the present study, instead of the descending curve pattern of normal pancreatic tissue, PET-positive tumors exhibited an ascending curve. However, the TACs of PET-negative tumors were similar to those of normal pancreatic tissue. Furthermore, there was a statistically significant difference between pNETs and RT in terms of K_i. A prospective study by Golan *et al.* (37) investigated dynamic ^{68}Ga-prostate-specific membrane antigen-11 PET-CT as a tool for the assessment of local renal masses and found that malignant renal masses showed greater tracer uptake and a slower washout compared to benign ones, as evidenced by distinct prostate-specific membrane antigen staining patterns. The study by Henze *et al.* (15) indicated that the uptake of ^{68}Ga-DOTATOC in meningiomas showed a biphasic response, with rapid increases during the first 10 min after tracer administration followed by slower increases during the remainder of the examination. In this study, the TAC characteristics of pancreatic head and tail lesions in patient 2 were similar to those of meningiomas, and the SUV_{max} and SUV_{mean} of these 2 lesions were also the highest. This was related to a continuous rise within 60 min without a plateau being reached.

An examination of the characteristics of meningiomas was conducted by Henze *et al.* (15) using dynamic ^{68}Ga-

DOTATOC PET, and significant differences were found between the SUV values of meningiomas and normal nasal mucosa (10.5 *vs.* 1.3; P<0.05). Although K_1 (0.54 *vs.* 0.40) was not significantly different, K_1:k_2 ratio was significantly higher in meningiomas than in RT (4.50 *vs.* 0.71). Consistent with literature reports, pNETs had significantly higher measures than did RT in terms of SUV_{max} (46.4 *vs.* 4.2; P=0.021), SUV_{mean} (21.9 *vs.* 2.7; P=0.036), and K_i (0.366 *vs.* 0.060; P=0.036). This study found that k_2 in pNETs was lower than in RT (2.076 *vs.* 2.939), and the K_1:k_2 ratio in pNETs was 12-fold higher than that in RT (6.06 *vs.* 0.50). We can conclude that the ^{68}Ga-DOTATATE uptake of pNETs can be explained by high K_i value and high K_1:k_2 ratio.

The study by Velikyan *et al.* (14) indicated that K_i might be a reliable indicator for quantifying SSTR expression and assessing treatment response. Perhaps this is due to the implicit consideration of plasma concentrations during the course of the scan when estimating K_i. Another study of ^{68}Ga-DOTATATE by Ilan *et al.* (38) reported tumor K_i for 12 patients with disseminated NETs undergoing therapy for variety of tumors (including small intestinal, pancreatic, rectal, and duodenal; grade 1–3). In comparison with the present study's K_i values, the K_i in pNETs was higher than the K_i in the disseminated NETs. K_i values in pNETs were within the range, of 0.019–0.992 (mean 0.366) as compared to the range, of 0.03–0.448 (mean 0.132) in disseminated NETs. The reason for these differences may be that the enrolled patients in our study had well-differentiated pNETs (grade 1 and grade 2) without any treatment before ^{68}Ga-DOTATATE PET-CT imaging. Additionally, the study found a positive correlation between K_i and tumor-to-blood ratio as well as between K_i and SUV in NETs according to ^{68}Ga-DOTATATE and ^{68}Ga-DOTATOC PET-CT (38). The same finding was also reported in another study (39), in which a positive correlation between K_{imax} and SUV_{max} was found, although ^{18}F-FDG was used as the imaging agent. Overall, our results are consistent with those of previous reports. This suggests that although SUV and K_i differ in quantitative SSTR expression, there is little doubt that both can be used for quantitative SSTR expression and that there is a positive correlation between them. A recent study by Yu *et al.* (25) demonstrated that SSTR2 immunohistochemistry could predict ^{68}Ga-DOTATATE PET-CT imaging accurately. The PET index in the study on the correlation between ^{68}Ga-SSA PET-CT and SSTR immunohistochemistry was the SUV derived from static imaging (25). Based on the positive correlation results of K_i with static imaging, we speculate that K_i and SSTR immunohistochemistry may also be related, and further exploration is needed in this field in the future.

In this study, a mass located in the tail of the pancreas was mistaken for a pNET due to contrast enhancement and enhanced ^{68}Ga-DOTATATE uptake characteristics. Postoperatively, the mass was diagnosed as IPAS. IPAS is characterized by a solid, contrast-enhancing mass that is usually in the tail of the pancreas and is smaller than 3 cm in diameter (40). It is therefore important to make an accurate diagnosis in order to avoid unnecessary surgery or biopsy. Similarly, physiological uptake of the pancreatic uncinate process is sometimes misdiagnosed as pNETs in ^{68}Ga-SSA PET-CT imaging. Recently, Thuillier *et al.* (21) reported excellent diagnostic performances of the K_i approach based on dynamic ^{68}Ga-DOTATOC PET-CT in identifying the physiological uptake of pancreatic uncinate process and pNETs. We will evaluate the possibility of dynamic ^{68}Ga-DOTATATE PET in further studies to help differentiate IPAS from pNETs.

This study also has some limitations. First, we used dynamic ^{68}Ga-DOTATATE PET-CT imaging to evaluate pathologically confirmed pNETs after surgical resection, and as patients without surgical pathological pNETs were not included, selection bias is possible. Second, immunostaining for SSTR2 and SSTR5 was performed for only 5 of 8 lesions, yet this was representative, considering the rarity of this tumor. Third, because most pNETs are in the late stage and there are relatively few cases with surgical indications, the enrolled cases in this study are relatively limited. Hence, the results should be regarded as preliminary. Finally, despite their widespread use in research settings, dynamic PET-CT protocols have not yet been widely adopted in clinical settings.

Conclusions

The value of dynamic ^{68}Ga-DOTATATE PET in pNETs can be summarized as follows: first, the TAC of pNETs mostly increases gradually with time; second, compared to RT, the uptake of ^{68}Ga-DOTATATE in pNETs is consistent with the high values for K_i and K_1:k_2 ratio; and finally, dynamic parameter K_i and static parameters SUV_{max}, SUV_{mean}, TPR, and TMR were all positively correlated. Pharmacokinetic modeling can thus serve as a potential tool for evaluating pNETs. These data may be useful for therapy planning and the monitoring of pNETs in a larger group of patients in future studies.

Acknowledgments

Funding: This study was funded by the National Key Research and Development Program of China (No. 2022YFC2406902 to HS), the Shanghai Municipal Key Clinical Specialty Project (No. SHSLCZDZK03401 to HS), the Major Science and Technology Projects for Major New Drug Creation (No. 2019ZX09302001 to HS), the Shanghai Science and Technology Committee Program (No. 20DZ2201800 to HS), the Three-year Action Plan of Clinical Skills and Innovation of Shanghai Hospital Development Center (No. SHDC2020CR3079B to HS), and the Next Generation Information Infrastructure Construction Project founded by the Shanghai Municipal Commission of Economy and Informatization (No. 201901014 to HS).

Footnote

Conflicts of Interest: All authors have completed the ICMJE uniform disclosure form (available at https://qims.amegroups.com/article/view/10.21037/qims-22-998/coif). The authors have no conflicts of interest to declare.

Ethical Statement: The authors are accountable for all aspects of the work in ensuring that questions related to the accuracy or integrity of any part of the work are appropriately investigated and resolved. This study was conducted in accordance with the Declaration of Helsinki (as revised in 2013). The study was approved by the institutional review board of Zhongshan Hospital (No. IRB-B2020-186R). All consecutive patients provided written informed consent before entering the study.

References

1. Hallet J, Law CH, Cukier M, Saskin R, Liu N, Singh S. Exploring the rising incidence of neuroendocrine tumors: a population-based analysis of epidemiology, metastatic presentation, and outcomes. Cancer 2015;121:589-97.
2. Dasari A, Shen C, Halperin D, Zhao B, Zhou S, Xu Y, Shih T, Yao JC. Trends in the Incidence, Prevalence, and Survival Outcomes in Patients With Neuroendocrine Tumors in the United States. JAMA Oncol 2017;3:1335-42.
3. Ma ZY, Gong YF, Zhuang HK, Zhou ZX, Huang SZ, Zou YP, Huang BW, Sun ZH, Zhang CZ, Tang YQ, Hou BH. Pancreatic neuroendocrine tumors: A review of serum biomarkers, staging, and management. World J Gastroenterol 2020;26:2305-22.
4. Ricci C, Casadei R, Taffurelli G, Campana D, Ambrosini V, Pacilio CA, Santini D, Brighi N, Minni F. Is radical surgery always curative in pancreatic neuroendocrine tumors? A cure model survival analysis. Pancreatology 2018;18:313-7.
5. Perri G, Prakash LR, Katz MHG. Pancreatic neuroendocrine tumors. Curr Opin Gastroenterol 2019;35:468-77.
6. Lestra T, Kanagaratnam L, Mulé S, Janvier A, Brixi H, Cadiot G, Dohan A, Hoeffel C. Measurement variability of liver metastases from neuroendocrine tumors on different magnetic resonance imaging sequences. Diagn Interv Imaging 2018;99:73-81.
7. Zilli A, Arcidiacono PG, Conte D, Massironi S. Clinical impact of endoscopic ultrasonography on the management of neuroendocrine tumors: lights and shadows. Dig Liver Dis 2018;50:6-14.
8. Hu HF, Hu YH, Xu XW, Ye Z, Lou X, Zhang WH, Chen XM, Zhang Y, Yu XJ, Gao HL, Xu JY, Ji SR. Role of Somatostatin Receptor 2 in Nonfunctional Pancreatic Neuroendocrine Tumors: Clinicopathological Analysis of 223 Cases and Whole Exome Sequencing of a Multifocal Case. Pancreas 2022;51:1404-10.
9. Gabriel M, Decristoforo C, Kendler D, Dobrozemsky G, Heute D, Uprimny C, Kovacs P, Von Guggenberg E, Bale R, Virgolini IJ. 68Ga-DOTA-Tyr3-octreotide PET in neuroendocrine tumors: comparison with somatostatin receptor scintigraphy and CT. J Nucl Med 2007;48:508-18.
10. Haug AR, Auernhammer CJ, Wängler B, Schmidt GP, Uebleis C, Göke B, Cumming P, Bartenstein P, Tiling R, Hacker M. 68Ga-DOTATATE PET/CT for the early prediction of response to somatostatin receptor-mediated radionuclide therapy in patients with well-differentiated neuroendocrine tumors. J Nucl Med 2010;51:1349-56.
11. Gabriel M, Oberauer A, Dobrozemsky G, Decristoforo C, Putzer D, Kendler D, Uprimny C, Kovacs P, Bale R, Virgolini IJ. 68Ga-DOTA-Tyr3-octreotide PET for

assessing response to somatostatin-receptor-mediated radionuclide therapy. J Nucl Med 2009;50:1427-34.
12. Meng QL, Yang R, Wu RZ, Xu L, Liu H, Yang G, Dong Y, Wang F, Chen Z, Jiang H. Evaluation of a respiratory motion-corrected image reconstruction algorithm in 2-[18F]FDG and [68Ga]Ga-DOTA-NOC PET/CT: impacts on image quality and tumor quantification. Quant Imaging Med Surg 2023;13:370-83.
13. Ma G, Du J, Zhang X, Liu J, Xu X, Xu B, Guan Z. Quantitative analysis of (68)Ga-DOTA(0)-Tyr(3)-octreotate positron emission tomography/computed tomography imaging for the differential diagnosis of primary pheochromocytoma and paraganglioma. Quant Imaging Med Surg 2022;12:2427-40.
14. Velikyan I, Sundin A, Sörensen J, Lubberink M, Sandström M, Garske-Román U, Lundqvist H, Granberg D, Eriksson B. Quantitative and qualitative intrapatient comparison of 68Ga-DOTATOC and 68Ga-DOTATATE: net uptake rate for accurate quantification. J Nucl Med 2014;55:204-10.
15. Henze M, Dimitrakopoulou-Strauss A, Milker-Zabel S, Schuhmacher J, Strauss LG, Doll J, Mäcke HR, Eisenhut M, Debus J, Haberkorn U. Characterization of 68Ga-DOTA-D-Phe1-Tyr3-octreotide kinetics in patients with meningiomas. J Nucl Med 2005;46:763-9.
16. Dimitrakopoulou-Strauss A, Georgoulias V, Eisenhut M, Herth F, Koukouraki S, Mäcke HR, Haberkorn U, Strauss LG. Quantitative assessment of SSTR2 expression in patients with non-small cell lung cancer using(68)Ga-DOTATOC PET and comparison with (18)F-FDG PET. Eur J Nucl Med Mol Imaging 2006;33:823-30.
17. Sandström M, Velikyan I, Garske-Román U, Sörensen J, Eriksson B, Granberg D, Lundqvist H, Sundin A, Lubberink M. Comparative biodistribution and radiation dosimetry of 68Ga-DOTATOC and 68Ga-DOTATATE in patients with neuroendocrine tumors. J Nucl Med 2013;54:1755-9.
18. Koukouraki S, Strauss LG, Georgoulias V, Eisenhut M, Haberkorn U, Dimitrakopoulou-Strauss A. Comparison of the pharmacokinetics of 68Ga-DOTATOC and 18FFDG in patients with metastatic neuroendocrine tumours scheduled for 90Y-DOTATOC therapy. Eur J Nucl Med Mol Imaging 2006;33:1115-22.
19. Koukouraki S, Strauss LG, Georgoulias V, Schuhmacher J, Haberkorn U, Karkavitsas N, Dimitrakopoulou-Strauss A. Evaluation of the pharmacokinetics of 68Ga-DOTATOC in patients with metastatic neuroendocrine tumours scheduled for 90Y-DOTATOC therapy. Eur J Nucl Med Mol Imaging 2006;33:460-6.
20. Ilan E, Sandström M, Velikyan I, Sundin A, Eriksson B, Lubberink M. Parametric Net Influx Rate Images of (68)Ga-DOTATOC and (68)Ga-DOTATATE: Quantitative Accuracy and Improved Image Contrast. J Nucl Med 2017;58:744-9.
21. Thuillier P, Bourhis D, Karakatsanis N, Schick U, Metges JP, Salaun PY, Kerlan V, Abgral R. Diagnostic performance of a whole-body dynamic 68GA-DOTATOC PET/CT acquisition to differentiate physiological uptake of pancreatic uncinate process from pancreatic neuroendocrine tumor. Medicine (Baltimore) 2020;99:e20021.
22. Breeman WA, de Jong M, de Blois E, Bernard BF, Konijnenberg M, Krenning EP. Radiolabelling DOTA-peptides with 68Ga. Eur J Nucl Med Mol Imaging 2005;32:478-85.
23. Moradi F, Jamali M, Barkhodari A, Schneider B, Chin F, Quon A, Mittra ES, Iagaru A. Spectrum of 68Ga-DOTA TATE Uptake in Patients With Neuroendocrine Tumors. Clin Nucl Med 2016;41:e281-7.
24. Skoura E, Michopoulou S, Mohmaduvesh M, Panagiotidis E, Al Harbi M, Toumpanakis C, Almukhailed O, Kayani I, Syed R, Navalkissoor S, Ell PJ, Caplin ME, Bomanji J. The Impact of 68Ga-DOTATATE PET/CT Imaging on Management of Patients with Neuroendocrine Tumors: Experience from a National Referral Center in the United Kingdom. J Nucl Med 2016;57:34-40.
25. Yu J, Cao F, Zhao X, Xie Q, Lu M, Li J, Yang Z, Sun Y. Correlation and Comparison of Somatostatin Receptor Type 2 Immunohistochemical Scoring Systems with 68Ga-DOTATATE Positron Emission Tomography/Computed Tomography Imaging in Gastroenteropancreatic Neuroendocrine Neoplasms. Neuroendocrinology 2022;112:358-69.
26. Diakatou E, Alexandraki KI, Tsolakis AV, Kontogeorgos G, Chatzellis E, Leonti A, Kaltsas GA. Somatostatin and dopamine receptor expression in neuroendocrine neoplasms: correlation of immunohistochemical findings with somatostatin receptor scintigraphy visual scores. Clin Endocrinol (Oxf) 2015;83:420-8.
27. Subramaniam RM, Bradshaw ML, Lewis K, Pinho D, Shah C, Walker RC. ACR Practice Parameter for the Performance of Gallium-68 DOTATATE PET/CT for Neuroendocrine Tumors. Clin Nucl Med 2018;43:899-908.
28. Okabayashi T, Shima Y, Sumiyoshi T, Kozuki A, Ito S, Ogawa Y, Kobayashi M, Hanazaki K. Diagnosis and management of insulinoma. World J Gastroenterol

2013;19:829-37.
29. Yu J, Ping F, Zhang H, Li W, Yuan T, Fu Y, Feng K, Xia W, Xu L, Li Y. Clinical Management of Malignant Insulinoma: a single Institution's experience over three decades. BMC Endocr Disord 2018;18:92.
30. Christ E, Antwi K, Fani M, Wild D. Innovative imaging of insulinoma: the end of sampling? A review. Endocr Relat Cancer 2020;27:R79-92.
31. Wild D, Christ E, Caplin ME, Kurzawinski TR, Forrer F, Brändle M, Seufert J, Weber WA, Bomanji J, Perren A, Ell PJ, Reubi JC. Glucagon-like peptide-1 versus somatostatin receptor targeting reveals 2 distinct forms of malignant insulinomas. J Nucl Med 2011;52:1073-8.
32. Peltola E, Vesterinen T, Leijon H, Hannula P, Huhtala H, Mäkinen M, Nieminen L, Pirinen E, Rönty M, Söderström M, Arola J, Jaatinen P. Immunohistochemical somatostatin receptor expression in insulinomas. APMIS 2023;131:152-60.
33. Nockel P, Babic B, Millo C, Herscovitch P, Patel D, Nilubol N, Sadowski SM, Cochran C, Gorden P, Kebebew E. Localization of Insulinoma Using 68Ga-DOTATATE PET/CT Scan. J Clin Endocrinol Metab 2017;102:195-9.
34. Falconi M, Eriksson B, Kaltsas G, Bartsch DK, Capdevila J, Caplin M, Kos-Kudla B, Kwekkeboom D, Rindi G, Klöppel G, Reed N, Kianmanesh R, Jensen RT; Vienna Consensus Conference participants. ENETS Consensus Guidelines Update for the Management of Patients with Functional Pancreatic Neuroendocrine Tumors and Non-Functional Pancreatic Neuroendocrine Tumors. Neuroendocrinology 2016;103:153-71.
35. Luo Y, Pan Q, Yao S, Yu M, Wu W, Xue H, Kiesewetter DO, Zhu Z, Li F, Zhao Y, Chen X. Glucagon-Like Peptide-1 Receptor PET/CT with 68Ga-NOTA-Exendin-4 for Detecting Localized Insulinoma: A Prospective Cohort Study. J Nucl Med 2016;57:715-20.
36. Wang Q, Wang RF, Zhang J, Zhou Y. Differential diagnosis of pulmonary lesions by parametric imaging in (18)F-FDG PET/CT dynamic multi-bed scanning. J BUON 2013;18:928-34.
37. Golan S, Aviv T, Groshar D, Yakimov M, Zohar Y, Prokocimer Y, Nadu A, Baniel J, Domachevsky L, Bernstine H. Dynamic (68)Ga-PSMA-11 PET/CT for the Primary Evaluation of Localized Renal Mass: A Prospective Study. J Nucl Med 2021;62:773-8.
38. Ilan E, Velikyan I, Sandström M, Sundin A, Lubberink M. Tumor-to-Blood Ratio for Assessment of Somatostatin Receptor Density in Neuroendocrine Tumors Using (68)Ga-DOTATOC and (68)Ga-DOTATATE. J Nucl Med 2020;61:217-21.
39. Fahrni G, Karakatsanis NA, Di Domenicantonio G, Garibotto V, Zaidi H. Does whole-body Patlak (18)F-FDG PET imaging improve lesion detectability in clinical oncology? Eur Radiol 2019;29:4812-21.
40. Bhutiani N, Egger ME, Doughtie CA, Burkardt ES, Scoggins CR, Martin RC 2nd, McMasters KM. Intrapancreatic accessory spleen (IPAS): A single-institution experience and review of the literature. Am J Surg 2017;213:816-20.

Cite this article as: Yin H, Liu G, Tan H, Shi D, Cheng D, Yu H, Shi H. Dynamic ^{68}Ga-DOTA^{0}-Tyr^{3}-octreotate positron emission tomography-computed tomography for the evaluation of pancreatic neuroendocrine tumors: a pilot study. Quant Imaging Med Surg 2023;13(9):5555-5567. doi: 10.21037/qims-22-998

